Physica D 291 (2015) 8–16

Contents lists available at ScienceDirect

Physica D

journal homepage: www.elsevier.com/locate/physd

Magnetisation oscillations by vortex–antivortex dipoles

Stavros Komineas *

Department of Applied Mathematics, University of Crete, 71409 Heraklion, Crete, Greece

HIGHLIGHTS

- The rotational dynamics of a magnetic vortex–antivortex dipole is studied.
- We produce a phase diagram by systematic numerical simulations.
- Three kinds of vortex–antivortex dipoles are identified, including merons.
- A virial relation and an asymptotic analysis give rotation frequency and stability.

ARTICLE INFO

Article history:
Received 11 July 2013
Received in revised form
3 July 2014
Accepted 3 October 2014
Available online 13 October 2014
Communicated by V.M. Perez-Garcia

Keywords:
Landau–Lifshitz equation
Magnetic vortex
Vortex–antivortex pairs
Spin-transfer oscillators
Merons

ABSTRACT

A vortex–antivortex dipole can be generated due to current with in-plane spin-polarisation, flowing into a magnetic element, which then behaves as a spin transfer oscillator. Its dynamics is analysed using the Landau–Lifshitz equation including a Slonczewski spin-torque term. We establish that the vortex dipole is set in steady state rotational motion due to the interaction between the vortices, while an external in-plane magnetic field can tune the frequency of rotation. The rotational motion is linked to the nonzero skyrmion number of the dipole. The spin-torque acts to stabilise the vortex dipole at a definite vortex–antivortex separation distance. In contrast to a free vortex dipole, the rotating pair under spin-polarised current is an attractor of the motion, therefore a stable state. The details of the rotating magnetisation configurations are analysed theoretically and numerically. The asymptotic behaviour of the rotating configurations provide results on their expected stability. Extensive numerical simulations reveal three types of vortex–antivortex pairs which are obtained as we vary the external field and spin-torque strength. We give a guide for the frequency of rotation based on analytical relations.

1. Introduction

The injection of a dc spin-polarised current through a magnetic element can induce magnetisation oscillations and thus turn a nanoelement into a spin-transfer-torque oscillator [1]. This property can be exploited for the design of, possibly, the smallest available frequency generators. The magnetisation configuration which is set in periodic motion may be a robust nonlinear magnetic excitation, such as a magnetic vortex, producing stable oscillations.

Magnetic vortices are typically seen to be created and annihilated in pairs in numerical simulations due to spin-polarised current [2–4]. In the experiments in Ref. [5] spin-polarised current was injected through an aperture into an elliptic-shaped magnetic element and magnetic oscillations were measured. Accompanying simulations showed a spontaneously nucleated vortex–antivortex (VA) pair, where vortex and antivortex have opposite polarities, in rotational motion.

The dynamics of vortex pairs has been previously studied in the context of the conservative Landau–Lifshitz (LL) equation [6–8]. Experimental and numerical results show that the creation and stabilisation of such VA pairs can occur under spin-polarised current, that is, in a non-conservative system driven by an external probe. The robustness of VA pairs in the excitable system is our motivation in order to study those in detail theoretically and numerically.

Magnetic solitons, in general, have already been studied for a long time, and a well-known class derives from the work of Belavin and Polyakov [9]. Their model is isotropic and allows for symmetric soliton configurations which are characterised by a topological charge, and also for configurations which possess one half unit of topological change, called *merons* [10]. A VA pair with opposite polarities, the object studied in this paper, can be viewed, topologically, as a two-meron configuration. However, we will use this term mostly for solutions with similar features to those of the original isotropic model. Earlier extensive work on magnetic solitons is reviewed in [11,12] where topological solitons and non-topological

* Tel.: +30 2810393732.
E-mail address: komineas@tem.uoc.gr.

http://dx.doi.org/10.1016/j.physd.2014.10.001
0167-2789/

magnetic droplets were studied. Some of these are dynamically stabilised. Recently, there is intensive activity on skyrmions which are observed in ferromagnets with an antisymmetric Dzyaloshinskii–Moriya interaction [13]. These are magnetic solitons with skyrmion number equal to unity. The VA dipoles studied in this paper possess the latter feature of skyrmions. We will call in the following a *skyrmion* any configuration with a nonzero skyrmion number.

Most of previous work on magnetic solitons was on a conservative system, with the possible addition of small damping. Unlike that work we study a non-conservative system with a damping mechanism and external driving. As a result we have many parameters (strength of spin-torque, external field, damping, etc.) and the system can be tuned to manifest multiple dynamical phenomena. On the other hand this complexity allows little space for an intuitive understanding of the phenomena based on existing lore. This difficulty is stressed by the number of experiments conducted, under different conditions, which have measured signals attributed to nonuniform or nonlinear magnetic states [14–16]. In the experiments in Ref. [5] it is counterintuitive that the VA pair performs a circular motion in the plane, while the polarisation of the spin current and the applied field point along a fixed in-plane direction, apparently breaking circular symmetry.

We will give a systematic theoretical and an extensive numerical study for vortex–antivortex dipoles in a current with in-plane spin-polarisation. This follows ideas already presented in Ref. [17]. We give a resolution of the mechanism for VA pair rotation which is necessary in order to understand the features of this system. We further give analytical formulae for the frequency of rotation which is then used as a guide to explore the behaviour of this system in its parameter space. Such a transparent qualitative and quantitative analysis of this multi-parameter system places previous results under a general framework and can be a guide for further experimental manipulation of the system and for the production of robust magnetisation oscillations.

The outline of the paper is as follows. In Section 2 we give the equation of motion. In Section 3 we give a general description of vortex–antivortex pairs and some analytical results. In Section 4 we give the results of numerical simulations. In Section 5 we give an asymptotic analysis of the rotating magnetisation configuration for large distances. In Section 6 we present rotating VA pairs for the special case of uniform spin-torque. Section 7 contains our concluding remarks. In Appendices A–C we give some background theoretical results and details of the numerical methods.

2. The Landau–Lifshitz–Gilbert–Slonczewski equation

The standard dynamics of the magnetisation vector $\boldsymbol{m} = (m_1, m_2, m_3)$ is given by the Landau–Lifshitz–Gilbert (LLG) equation. A spin-polarised current is assumed to flow through an ultrathin film inducing excitation of the magnetisation which can be described by an additional, so called, Slonczewski spin-torque term in the LLG equation [18] (see [19] for a review). The model which will be used throughout this paper is the Landau–Lifshitz–Gilbert–Slonczewski (LLGS) equation, in rationalised form,

$$\dot{\boldsymbol{m}} = -\boldsymbol{m} \times (\alpha_1 \boldsymbol{f} - \alpha_2 \beta\, \boldsymbol{p}) - \boldsymbol{m} \times [\boldsymbol{m} \times (\alpha_2 \boldsymbol{f} + \alpha_1 \beta\, \boldsymbol{p})]$$
$$\boldsymbol{f} \equiv \Delta \boldsymbol{m} - m_3 \hat{\boldsymbol{e}}_3 + \boldsymbol{h}_{\rm ext}. \tag{1}$$

Damping is accounted for by the coefficients $\alpha_1 = 1/(1+\alpha^2)$, $\alpha_2 = \alpha/(1+\alpha^2)$, where α is the Gilbert dissipation constant. We have taken into account three terms in the effective field $\boldsymbol{f}$: the exchange interaction, an easy-plane anisotropy term perpendicular to the third magnetisation direction $\hat{\boldsymbol{e}}_3 = (0, 0, 1)$, and an external field $\boldsymbol{h}_{\rm ext}$. The spin-polarisation of the current is along the direction $\boldsymbol{p}$ which is taken to be a constant vector. We further assume that the coefficient of the spin-torque term β is a constant, thus we confine ourselves to studying a simple form of the spin-torque term.

We consider Eq. (1) as a two-dimensional model, that is, the magnetisation is a function of two spatial variables and time, $\boldsymbol{m} = \boldsymbol{m}(x, y, t)$. This is assumed to be the limit of an ultrathin film, and the easy-plane anisotropy term is considered mainly as an approximation to the magnetostatic energy.

The magnetisation $\boldsymbol{m}$ and the field $\boldsymbol{h}_{\rm ext}$ are measured in units of the saturation magnetisation M_s, so $\boldsymbol{m}^2 = 1$. The units of length and time are, respectively,

$$\ell_{\rm ex} \equiv \sqrt{\frac{2A}{\mu_0 M_s^2}}, \qquad \tau_0 = (\gamma \mu_0 M_s)^{-1}, \tag{2}$$

where A is the exchange constant, γ is the gyromagnetic ratio, and $\ell_{\rm ex}$ is the exchange length. The spin-torque parameter β is defined as

$$\beta = \frac{J_{\rm e}}{J_{\rm p}}, \quad J_{\rm p} = \frac{\mu_0 M_s^2 |e| d_f}{\hbar}, \tag{3}$$

where $J_{\rm e}$ is the current density and d_f is the thickness of the film. For permalloy we have $\ell_{\rm ex} \approx 7$ nm, and $\tau_0 \approx 7$ ps which corresponds to a frequency $f_0 = 1/(2\pi\,\tau_0) \approx 23$ GHz, and typically $J_{\rm p} \approx 3 \times 10^{12}$ A/m^2.

We consider a ferromagnetic state $\boldsymbol{m}_0 = (1, 0, 0)$. Such a magnetisation orientation may be due to the shape of the film, as in the case of the elliptic samples in Ref. [5], or it may be imposed through the application of an external magnetic field. The polarisation $\boldsymbol{p}$ of the current is assumed

$$\beta\, \boldsymbol{p} = \beta\, (1, 0, 0), \quad \beta < 0, \tag{4}$$

that is, it forces the magnetisation antiparallel to $\boldsymbol{m}_0$. Following experimental setups we mostly assume that the current flows through a nano-aperture with a diameter of tens of nanometres. However, we also study the case of uniform spin current in Section 6. Whenever an external magnetic field is present this is considered uniform and has the form

$$\boldsymbol{h}_{\rm ext} = (h_{\rm ext}, 0, 0), \quad h_{\rm ext} > 0, \tag{5}$$

that is, it favours the ferromagnetic state $\boldsymbol{m}_0$.

3. Steady-state rotating dipoles

3.1. Vortex–antivortex pair

Vortices are magnetisation configurations where the magnetisation vector rotates a full 2π angle when a circle is traced around a point called the vortex centre. They are thus characterised by a *winding number* $\kappa = \pm 1$. The positive value corresponds to the vortex typically observed in magnetic elements, which minimises the magnetostatic energy. A vortex with a negative winding number is called an antivortex. Easy-plane anisotropy supports vortices with their *polarity* along the third axis taking the two values $\lambda = \pm 1$.

A configuration of a VA pair has been conjectured to form during dynamical processes in experiments, and the process has been demonstrated numerically. We will study only the case where the vortex and the antivortex have opposite polarities. Such a VA dipole has a nonzero skyrmion number. The latter is defined as

$$\mathcal{N} = \frac{1}{4\pi} \int n\, d^2x, \quad n = \frac{1}{2} \epsilon_{\mu\nu} (\partial_\nu \boldsymbol{m} \times \partial_\mu \boldsymbol{m}) \cdot \boldsymbol{m}, \tag{6}$$

where n is a local topological density and $\epsilon_{\mu\nu}$ is the totally antisymmetric tensor with $\mu, \nu = 1, 2$ [20]. A VA dipole has $\mathcal{N} = \pm 1$. We conventionally take the vortex with negative polarity and the

antivortex with positive polarity, so the pair has $\mathcal{N} = 1$. Changing the polarities of both vortices would change the sign of $\mathcal{N}$.

Due to the interaction between the two vortices the pair cannot be static. The vortices rotate clockwise or anticlockwise depending on the sign of $\mathcal{N}$. The situation is clear within the conservative LL equation, i.e., Eq. (1) for $\alpha = 0, \beta = 0$ and no external field $\boldsymbol{h}_{\rm ext} = 0$. The pair is pinned at the position where it is created and their dynamics is rotational [6]. This can be linked to the nonzero skyrmion number [8] and the vortices rotate clockwise or anticlockwise depending on the sign of $\mathcal{N}$. It is seen numerically that their motion can be close to a steady state rotation, however, this appears to be unstable. If we add dissipation $\alpha \neq 0$ to the model then the vortices go on a spiralling orbit towards each other.

The rotational motion is stable in the case of a VA dipole under the influence of a spin-polarised current flowing through a thin magnetic element, as shown in experiments and simulations [5,17]. The extensive numerical simulations in Section 4 show that the rotational motion is a stable steady state for a range of parameter values. We stress that both the current polarisation (4) and the external field (5) will be considered to be in-plane, along the x-axis. In such a case one would, in general, expect precession of the magnetisation around the x axis. So, the observed rotation is not easily interpreted as a straightforward consequence of the precessional dynamics of the Landau–Lifshitz equation.

A simple ansatz for a VA dipole can be written through the stereographic variable discussed in Appendix A. The form (A.5) represents a VA configuration which is an exact solution of the LL equation when only the exchange interaction is considered. The roles of the external magnetic field and the spin-torque term manifest themselves explicitly in this case [17]. The spin-torque acts to stabilise the radius of rotation while the external field gives the angular frequency of rotation. The rotation frequency is inversely proportional to the skyrmion number, which shows that it is crucial that $\mathcal{N} \neq 0$ for these results to be valid.

3.2. Virial relation

Based on the evidence from numerics we conjecture the existence of a magnetic configuration in steady-state rotation, in the sense of Eq. (B.1). The approximation of a steady-state allows for the derivation of explicit results. Appendix B details a virial relation of Derrick type given in Eq. (B.2) which is exact in the case of steady-state rotation. According to the results of numerical simulations a simplified form of the Derrick relation (B.2) holds to a very good approximation for most of the VA dipoles presented in this paper. This gives the angular velocity of rotation as

$$\omega \doteq -\left(\frac{E_{\rm a}}{\ell} + h_{\rm ext}\frac{\mu_1}{\ell}\right), \tag{7}$$

where the symbol $\doteq$ indicates an approximation. The quantity

$$\ell = \frac{1}{2}\int \rho^2\, n\, d^2x, \quad \rho^2 \equiv x_1^2 + x_2^2, \tag{8}$$

defined through the topological density n, is identified with the angular momentum [21]. For a VA pair with well-separated vortex and antivortex at a distance $d_{\rm VA}$, we can readily write the approximate formula $\ell \approx (\pi/2)\mathcal{N} d_{\rm VA}^2$. We will actually define the vortex–antivortex distance (for $\mathcal{N} = 1$) as

$$d_{\rm VA} \equiv \sqrt{\frac{2\ell}{\pi}}. \tag{9}$$

The quantity

$$E_{\rm a} = \frac{1}{2}\int (m_3)^2\, d^2x \tag{10}$$

is the anisotropy energy, which takes the value $E_{\rm a} = \pi/2$ for a single isolated vortex [22]. We have also defined

$$\mu_1 = -\frac{1}{2}\int x_\mu \partial_\mu m_1\, d^2x = \int (1 - m_1)\, d^2x, \tag{11}$$

where the last equation derives from a partial integration assuming vanishing boundary terms, and the final quantity gives the total magnetisation (spin reversals) in the x axis.

Eq. (7) is derived from Eq. (B.2) if we neglect two terms. The term proportional to the dissipation constant α is neglected because the dissipation constant itself is small. The term proportional to β is neglected because the corresponding integral is small. For example, one could use the configuration (A.4), which gives a VA pair perfectly symmetric around an in-plane axis, to find that the last integral in the Derrick relation (7) vanishes. The small values for the integral actually found in the simulations are due to small asymmetries of the rotating VA pairs. Finally, we note that these arguments do not fully justify the approximation in Eq. (7), but this is rather supported by the numerical results, given later in the paper.

Relation (7) establishes that the angular frequency of a rotating VA pair has contributions from two separate sources. The first term on the right hand side is due to the interaction between the vortex and the antivortex. This decreases as the distance between the vortices increases (ℓ increases). The second term on the right hand side of (7) is due to the external field and it includes a factor which depends on the details of the magnetisation configuration. It is crucial for both terms that $\mathcal{N} \neq 0$, since otherwise the quantity ℓ could vanish and change completely the meaning of the Derrick relation.

4. Numerical simulations

4.1. Magnetisation configurations

We have performed a series of numerical simulations based on Eq. (1). They are performed in two dimensions using stretched coordinates for the infinite plane. The details of the method are given in Appendix C. Following experiments we assume that the spin current is injected in the nanoelement through an aperture. We model the flow of the current through a nano-aperture by assuming a spin-torque parameter $\beta \neq 0$ in a disc with diameter $d_a \approx 40$ nm while we set $\beta = 0$ outside it. For spin polarisation as in Eq. (4) numerical simulations [5] have shown that the spin-torque causes the magnetisation to switch at the central area of the element and finally induces the generation of a VA dipole in rotational motion around the centre of the spin current. Mechanisms for the generation of a VA dipole are presented by numerical simulations in Ref. [4]. In the present paper we *assume* the existence of a vortex dipole and study its subsequent dynamics.

As the number of parameters in the present problem is large we will not explore all possibilities but we will rather fix the values

$$\alpha = 0.02, \qquad d_a = 6\ell_{\rm ex}, \tag{12}$$

for the dissipation constant and the aperture diameter respectively. Numerical simulations performed with similar values for α have given quantitatively similar results. Other values for d_a (e.g., $d_a = 4\ell_{\rm ex}$ and $12\ell_{\rm ex}$) did not give qualitatively different results. However, more extensive simulations would be needed in order to explore the dependence of results on d_a.

We evolve in time an initial ansatz for a VA pair configuration according to the LLGS equation (1) and this typically converges to a steady-state rotating VA pair. As the same result is obtained for any initial condition that we used (see Appendix C), we conclude that these are stable dynamical magnetic configurations.

We study the features of our system by systematically varying the parameters which can be tuned experimentally: the externally

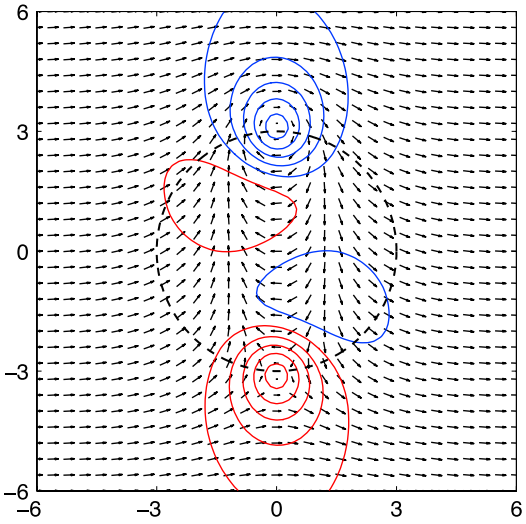

Fig. 1. Magnetisation configuration of type I (long VA pair) for vortex–antivortex pair in steady-state rotation around a nano-aperture (delimited by a dashed line). The vector plot shows (m_1, m_2) and the contour plot is for the perpendicular magnetisation component. We plot contour levels $m_3 = \pm 0.1, \pm 0.3, \pm 0.5, \pm 0.7, \pm 0.9$ (red: up, blue: down). Parameter values used are $\beta = -0.10$, $h_{\text{ext}} = 0.40$ and (12). The angular frequency of rotation is $\omega = 0.255$. (For interpretation of the references to colour in this figure legend, the reader is referred to the web version of this article.)

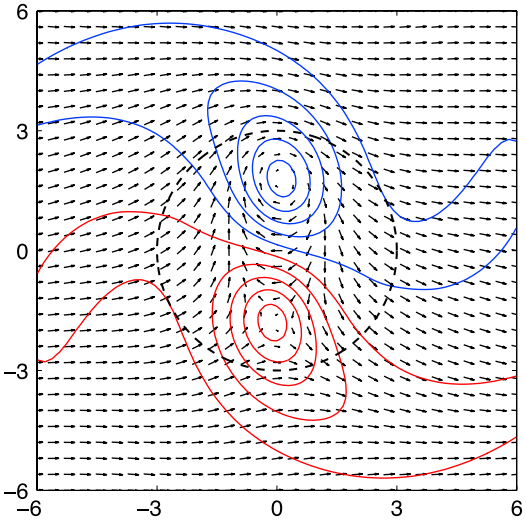

Fig. 2. Magnetisation configuration of type II (short VA pair) in steady-state rotation. We plot as in Fig. 1. Parameter values used are $\beta = -0.10$, $h_{\text{ext}} = 0.40$ (the same as in Fig. 1). The angular frequency of rotation is $\omega = 0.539$.

applied field h_{ext} and the strength of the spin current β. We start by choosing a typical value for the current $\beta = -0.1$. We then vary the external field and find a series of rotating VA pairs. Varying h_{ext} from the value $h_{\text{ext}} = 0$ up to $h_{\text{ext}} = 0.44$ we find configurations similar in form to that shown in Fig. 1 for the specific value $h_{\text{ext}} = 0.4$. We label these VA pairs of type I (or *long* VA pairs) and note that the vortex and antivortex are well separated.

Varying h_{ext} from larger to smaller values we find configurations similar in form to that shown in Fig. 2 for the value $h_{\text{ext}} = 0.4$. We label these VA pairs of type II (or *short* VA pairs). Note that the two VA pairs shown in Figs. 1, 2 are obtained for the same parameter values, but they are different and they have significantly different rotation frequencies.

Increasing the spin current to $\beta = -0.2$ and choosing large external field values we find still one more kind of VA pairs, shown in Fig. 3 for the value $h_{\text{ext}} = 0.6$. We label these VA pairs of type III (or *wide* VA pairs).

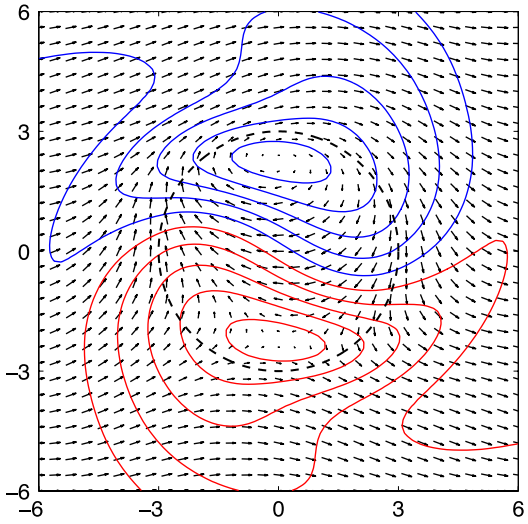

Fig. 3. Magnetisation configuration of type III (wide VA pair) in steady-state rotation. We plot as in Fig. 1. Parameter values used are $\beta = -0.20$, $h_{\text{ext}} = 0.60$. The angular frequency of rotation is $\omega = 0.820$.

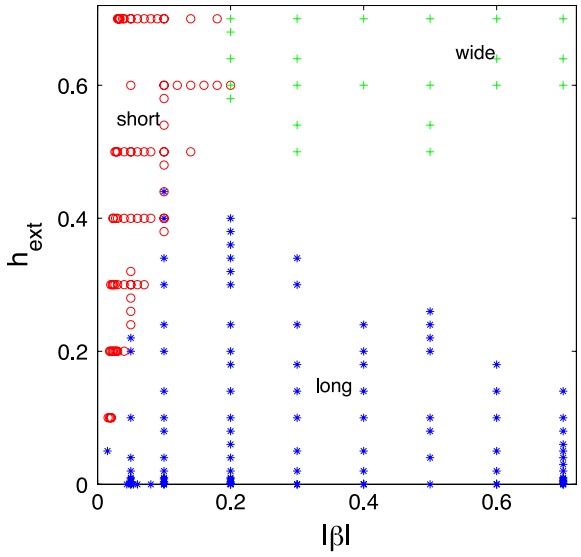

Fig. 4. Numerical simulations have given three types of rotating VA pairs. In the β–h_{ext} plane we plot blue stars for type I (long) pairs, red circles for type II (short) VA pairs, and green crosses for type III (wide) VA pairs. No steady-states were found in the regions where no symbols are plotted: (i) for very small β values and (ii) for large β and intermediate h_{ext}. Other parameters are as in Eq. (12).

We have explored systematically the range of parameters $0 \leq |\beta| \leq 0.7$ and $0 \leq h_{\text{ext}} \leq 0.7$. We find the three types of VA pairs in steady-state rotation on the β–h_{ext} plane as shown in Fig. 4. Each symbol corresponds to a numerical simulation which has successfully converged to a VA pair rotating in a steady-state. Stars correspond to long VA pairs, circles to short pairs and crosses to wide pairs. There are small regions in the parameter space where more than one type of VA pairs has been found. We obtain one or the other configuration depending on the initial condition used or on the direction of sweeping the parameter space. For the parameter values where we have both a long and a short VA pair, the choice of Eq. (A.5) as an initial condition gives a short VA pair while well separated vortex and antivortex as an initial condition gives a long VA pair.

In a significant word of caution we mention that our simulations do not prove that the calculated states represent exact steady-states. While most of these seem to be exact within our numerical

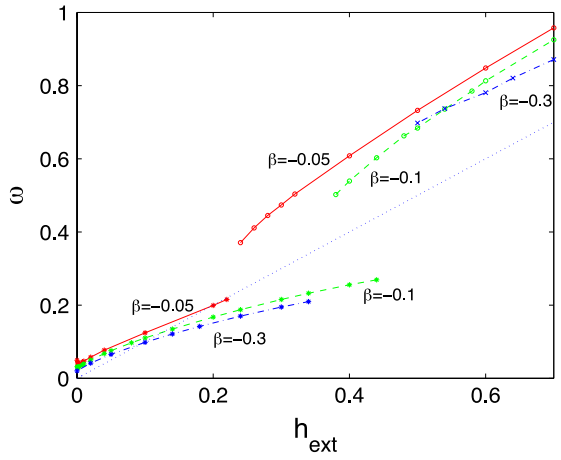

Fig. 5. Angular frequency ω of rotation (absolute value) as a function of external field h_{ext} for three fixed values of the current density $\beta = -0.05$ (solid-red line), $\beta = -0.1$ (dashed-green line), and $\beta = -0.3$ (dashed–dotted-blue line). Symbols correspond to actual simulation results. Stars denote long VA pairs, circles denote short pairs, and crosses denote wide pairs. The frequency ω goes to a nonzero value for $h_{\text{ext}} = 0$. There is a jump in the frequency when we change from long to short or wide pairs. For $\beta = -0.1$ two types of VA pairs coexist for a range of h_{ext} values. The dotted line shows $\omega = h_{\text{ext}}$ for comparison purposes.

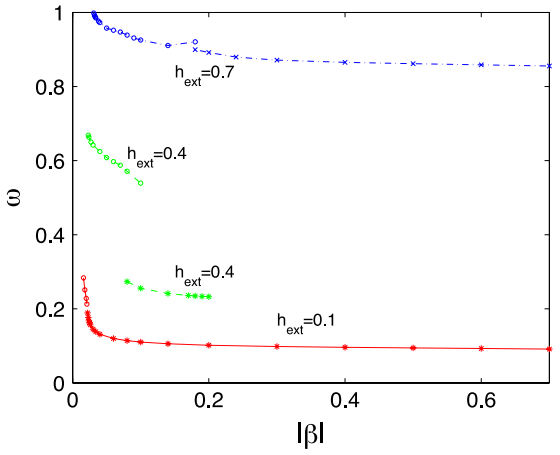

Fig. 6. Angular frequency ω of rotation as a function of spin-torque β for three fixed values of the external field $h_{\text{ext}} = 0.1$ (solid-red line), $h_{\text{ext}} = 0.4$ (dashed-green line), and $h_{\text{ext}} = 0.7$ (dashed–dotted-blue line). Stars denote long VA pairs, circles denote short pairs, and crosses denote wide pairs. There is a jump in the frequency when we change from long to short or to wide pairs in all case, but it is much more pronounced for $h_{\text{ext}} = 0.4$. No VA pairs are sustained for very small values of $|\beta|$. The frequency ω increases sharply for small β and is nearly saturated for large spin-torque values.

accuracy, in some others we measure small fluctuations. Especially the wide pairs for smaller h_{ext} show fluctuations ∼1%–3% in various quantities calculated numerically.

A test for our theoretical and numerical results is provided by comparing the Derrick relation (B.2) against numerical results. The Derrick relation is used to find the angular frequency ω and we find that this agrees to an accuracy better than 1% with the measured angular frequency for most of our simulations. The discrepancy is larger (up to 4%) in the cases that fluctuations are observed in the rotation.

In the areas in Fig. 4 where no symbols are plotted we have found no steady-state rotating VA pairs. Instead, the simulations give dynamical states which do include a VA dipole in rotation, but the motion is accompanied by a continuous creation and annihilation of more VA pairs with same polarities. We will not refer any further to these dynamical states in the present paper. Simulations and studies of similar states in a related system have been given in Refs. [4,3].

Finally, we refer to recent work [23] where non-symmetric solitons are stabilised due to conservation of orbital moment, while the possibility of existence of different stable solitons simultaneously has been demonstrated. Of course, the models here and in [23] are different, but both have an integral of motion.

4.2. Frequency of rotation

For a more detailed presentation of results we fix the spin-torque parameter β and vary the field h_{ext}. In Fig. 5 we present the angular frequency ω of VA pair rotation for three fixed values of the spin-torque and for external field values in the range $0 \le h_{\text{ext}} \le 0.7$. For $\beta = -0.1$ and $0 \le h_{\text{ext}} \le 0.44$ we find long VA pairs while for $0.38 \le h_{\text{ext}} \le 0.7$ we find short VA pairs. The transition between the two kind of VA pairs is not smooth, the magnetic configuration and the angular frequency change significantly. Furthermore, the two types of VA pairs coexist for the range $0.38 \le h_{\text{ext}} \le 0.44$. For $\beta = -0.05$ there is a small gap in the range of h_{ext} where no steady-state rotating VA pairs are found. For $\beta = -0.3$ we have long pairs for small h_{ext}, wide pairs for large h_{ext} and no steady states for a range of h_{ext} in between. VA pairs are certainly stable also for $h_{\text{ext}} = 0$ and they are rotating at a nonzero ω.

We continue by fixing $h_{\text{ext}} = 0.1$ and varying β. In Fig. 6 we present the angular frequency ω of rotation for three values of h_{ext} and for spin-torque in the range $0 \le |\beta| \le 0.7$. For $h_{\text{ext}} = 0.1$ we find long VA pairs for $0.022 \le |\beta| \le 0.7$ and short VA pairs for $0.016 \le |\beta| \le 0.21$. The transition between the two kinds of VA pairs is not smooth, and the angular frequency jumps. This becomes completely obvious for $h_{\text{ext}} = 0.4$ where we have a significant jump to higher frequencies for short VA pairs at $|\beta| \approx 0.1$. For the values $0.08 \le |\beta| \le 0.1$ both long and short pairs are found. For $h_{\text{ext}} = 0.7$ we have short VA pairs for smaller $|\beta|$ values and wide pairs for larger values of the spin-torque.

It appears straightforward to understand the long VA pairs as a combination of a vortex and an antivortex which are well-separated but still interacting. This is in accordance with the overall configuration but also with the detailed features obtained in the simulations. For example, the anisotropy energy of long VA pairs is roughly twice that of a single isolated vortex, i.e., $E_{\text{a}} \approx \pi$. The short as well as the wide VA pairs are characterised by the fact that their magnetisation is roughly similar to their angular momentum, i.e., $\mu_1 \approx \ell$. This is a feature present in two-meron configurations of the pure exchange model [10,17]. The short and the wide VA pairs thus appear to be related to those two-meron configurations, except that, unlike merons such as in Eq. (A.5), the VA dipole configuration decays exponentially to the ground state at large distances and is thus well-localised. The wide VA pairs have a large anisotropy energy $E_{\text{a}} \sim 15$–20, which is many times larger than the anisotropy energy of two isolated vortices. Short VA pairs have anisotropy energy in the range $E_{\text{a}} \sim 3$–6. Short and wide VA pair seem to have some similarities, however, based on the results presented here they cannot be considered as the same type. For example, for $h_{\text{ext}} = 0.6$, $\beta = -0.2$ we find both types.

In some cases we can have approximations for ω directly derived from the virial relation (7). For the case of very small external field the vortex and antivortex are well separated, so we can use the approximation $E_{\text{a}} \approx \pi$ and Eq. (9). Then, the virial relation for long VA pairs, in the case $h_{\text{ext}} \ll 1$, gives

$$\omega \approx \frac{2}{d_{\text{VA}}^2}. \tag{13}$$

In Fig. 7 we show ω vs. β for $h_{\text{ext}} = 0$ and compare numerical results against the approximation in Eq. (13). In the latter formula, we substitute for d_{VA} the distance between the points where $m_3 = \pm 1$ (centres of vortices), as this formula is only considered as an intuitive rough guide for ω.

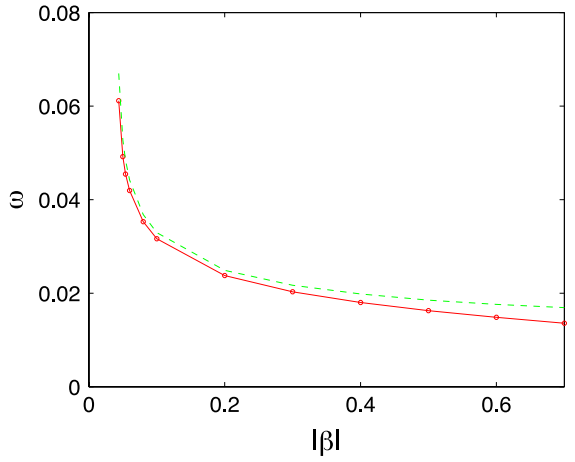

Fig. 7. Angular frequency of rotation ω (absolute value) as a function of $|\beta|$ for $h_{\text{ext}} = 0$. The simulation results (solid-red line, symbols correspond to actual simulation results) are compared with the approximation (dashed-green line) given in Eq. (7).

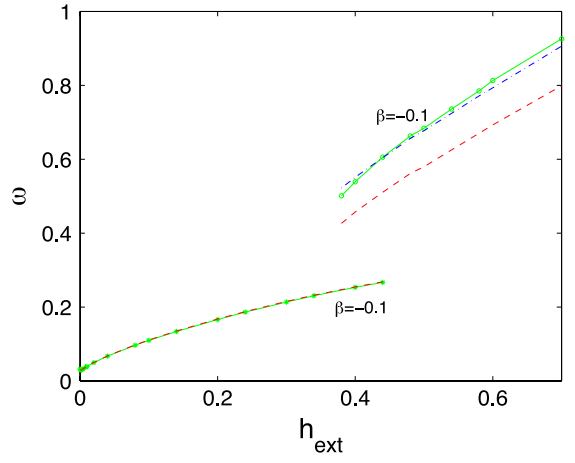

Fig. 8. Angular frequency ω of rotation (absolute value) as a function of external field h_{ext} for $\beta = -0.1$ (solid-green line), is compared to the result from the approximate virial relation (7) (dashed-red line). Also, the result from the approximation in Eq. (14) is plotted for short VA pairs (dash-dotted blue line).

For long VA pairs at external fields $h_{\text{ext}} > 0.1$ we find in simulations $\ell > \mu_1$. Therefore, the virial relation (7) indicates an angular frequency $\omega < 2/d_{\text{VA}}^2 + h_{\text{ext}}$.

Short VA pairs appear for larger external fields. Since $\mu_1 \approx \ell$ the Derrick relation gives

$$\omega \approx \frac{E_{\text{a}}}{\ell} + h_{\text{ext}}. \tag{14}$$

The first term on the right hand side depends on the precise form of the magnetic configuration. The approximations given before Eq. (13) are not very good any more, however, one could still use them as a rough guide obtaining a contribution $\sim 2/d_{\text{VA}}^2$ to the angular frequency. Approximation (14) is valid for wide VA pairs, too, for which we also have $\mu_1 \approx \ell$. These VA pairs have large anisotropy energy $E_{\text{a}} \sim$ 15–20 and also larger angular momentum ℓ. Their angular frequency ω tends to be similar to that for short VA pairs at similar h_{ext} values as seen in Fig. 6.

Fig. 8 shows ω vs. h_{ext} for a specific value of spin-torque $\beta = -0.1$ and gives a comparison with the Derrick relation (7). The approximation is excellent for long VA pairs. The discrepancy observed for short VA pairs is mostly due to the term proportional to the dissipation constant α in the full Derick relation (B.2) which was neglected in the approximation (7). The same figure compares

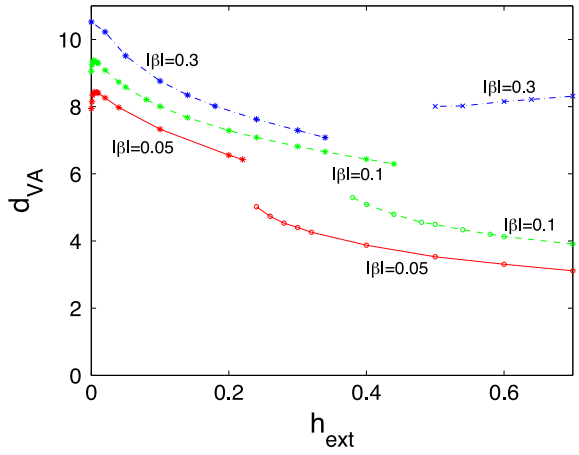

Fig. 9. Separation distance between vortex and antivortex defined in Eq. (9) as a function of external field h_{ext} for three fixed values of the current density $\beta = -0.05$ (solid-red line), $\beta = -0.1$ (dashed-green line), and $\beta = -0.3$ (dashed–dotted-blue line). Stars denote long VA pairs, circles denote short VA pairs, and crosses denote wide pairs. The magnetic field favours the ground state so it acts to shrink the VA pairs, i.e., decrease d_{VA}. The sharp change for d_{VA} for very small $h_{\text{ext}} < 0.01$ is discussed in Section 5.

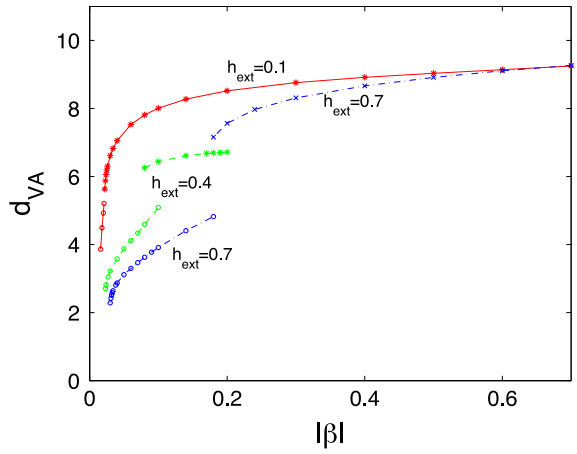

Fig. 10. Separation distance between vortex and antivortex defined in Eq. (9) as a function of spin-torque β for three fixed values of the external field $h_{\text{ext}} = 0.1$ (solid-red line), $h_{\text{ext}} = 0.4$ (dashed-green line), and $h_{\text{ext}} = 0.7$ (dashed–dotted-blue line). Stars denote long VA pairs, circles denote short VA pairs, and crosses denote wide pairs. For very small $|\beta|$ no VA pairs are sustained. The vortex and antivortex come closer for small $|\beta|$, and d_{VA} saturates for large $|\beta|$.

numerical results of short VA pairs with the approximation (14). We would expect that Eq. (7) is a better approximation than Eq. (14). Fig. 8 shows that the opposite happens, but this is apparently a coincidence.

A quantity of potential interest for experimental work and applications is the distance d_{VA} between vortex and antivortex defined in Eq. (9). Fig. 9 shows d_{VA} as a function of h_{ext} for three values of β. Larger values of h_{ext} tend to make the VA pair shrink, as h_{ext} favours the ground state. Fig. 10 shows d_{VA} as a function of β for three values of external field h_{ext}. The main features are that (i) d_{VA} saturates for strong spin torque and (ii) the vortex and antivortex come very close together for small β values or for large h_{ext}.

VA dipoles are sustained even for quite small values of β. Smaller $|\beta|$ gives smaller VA pairs and larger ω. For very small values of $|\beta|$ below a certain threshold (which depends on h_{ext}, as can be seen in Fig. 4) the simulations show collapse of any initial configuration to the ground state. An estimation for the maximum possible ω is given in Section 5.

5. Asymptotics for large distances

Some features of the profiles of the magnetisation for rotating VA pairs can be found by looking into their asymptotic behaviour at large distances from the pair. Conclusions will be drawn which elucidate some elements of the picture found by numerical simulations in Section 4. In particular, we can study the decay of the magnetisation profile to the ferromagnetic state at large distances from the VA pair as we expect that localisation properties of the configuration could play a significant role in its stability.

All calculations are conveniently performed using the stereographic variable defined in Eq. (A.1). We are interested in configurations for which $X(\rho \to \infty) \to 0$, so we linearise (A.3) and we use polar coordinates (ρ, ϕ). We are interested in steady rotational motion, so we assume $\dot{X} = -\omega \partial_\phi X$. The linearised form of (A.3), with the latter substitution, is

$$\left(\partial_\rho^2 X + \frac{\partial_\rho X}{\rho} + \frac{\partial_\phi^2 X}{\rho^2}\right) - \frac{1}{2}(X - \overline{X}) - (h_{\text{ext}} + i\beta) X + \omega(i + \alpha)\, \partial_\phi X = 0. \tag{15}$$

Solutions can be found by writing X as a Fourier series:

$$X(\rho, \phi) = \sum_{n=-\infty}^{\infty} X_n(\rho)\, e^{in\phi}, \tag{16}$$

where X_n are complex functions of ρ. Substituting (16) in (15) we obtain a linear system of differential equations for the X_n's. In order to find solutions we assume that X_n satisfies Bessel equation

$$\left(\partial_\rho^2 + \frac{\partial_\rho}{\rho} - \frac{n^2}{\rho^2}\right) X_n = -(\kappa_1 + i\kappa_2) X_n, \tag{17}$$

where we have introduced a complex eigenvalue $\kappa_1 + i\kappa_2$. So we write

$$X_n(\rho) \sim X_n^0\, H_n\left(\sqrt{\kappa_1 + i\kappa_2}\, \rho\right), \tag{18}$$

where X_n^0 are complex constants and H_n are Hankel functions [24,25].

Substituting the form (18) in the system of differential equations for X_n we obtain an algebraic system which is closed for every pair of unknowns X_n^0, X_{-n}^0. The characteristic equation for the system is

$$\begin{vmatrix} -(K_1 + n\omega) - iK_2 & \frac{1}{2} \\ \frac{1}{2} & -(K_1 - n\omega) - iK_2 \end{vmatrix} = 0, \tag{19}$$

where $K_1 \equiv \kappa_1 + h_{\text{ext}} + 1/2$ and $K_2 \equiv \kappa_2 - n\alpha\omega$. Note that β does not appear in this condition as we consider here the case where the spin-torque term is localised around the origin and is therefore zero at large distances. We find

$$\kappa_1 = \kappa_\pm \equiv -\left(\frac{1}{2} + h_{\text{ext}}\right) \pm \sqrt{\frac{1}{4} + (n\omega)^2} \tag{20}$$

$$\kappa_2 = n\alpha\omega.$$

We focus on the behaviour of the Hankel functions at large distances ($\rho \to \infty$), which is given by

$$H_n(z) \sim \sqrt{\frac{2}{\pi z}}\, e^{\pm i\left(z - \frac{n\pi}{2} - \frac{\pi}{4}\right)}, \tag{21}$$

where $z \equiv (\lambda_1 + i\lambda_2)\, \rho$ with $\lambda_1 + i\lambda_2 = \sqrt{\kappa_1 + i\kappa_2}$. For a decaying profile we should choose the sign for which the exponent is negative. The component for $n = 1$ corresponds to a VA pair, and such an example is given in Eq. (A.5). In view of the solutions studied in this paper we assume that the component for $n = 1$ is prevailing at $\rho \to \infty$ over components with $n > 1$, which would give multiple VA pair configurations. So, we require that the decay in Eq. (21) should be slowest for $n = 1$, in view of the solutions we study in this paper: these are skyrmion solutions, e.g., as in Eq. (A.5).

We set $n = 1$ in Eq. (20) and obtain

$$\lambda_1 = \frac{1}{2}\frac{\alpha\omega}{\lambda_2}$$
$$\lambda_2 = \sqrt{\frac{-\kappa_1 + \sqrt{\kappa_1^2 + (\alpha\omega)^2}}{2}}. \tag{22}$$

The main features of the asymptotic solutions and, consequently, some properties of the full magnetisation profiles depend on the eigenvalues, $\lambda_{1,2}$ in Eq. (22). The values of these quantities are found provided the angular frequency ω is known from the simulations.

The case $\kappa_1 = \kappa_+$ is the most interesting because it gives a smaller value for λ_2 and thus slower decay in Eq. (21). A case of special interest occurs when $\kappa_1 \geq 0$ because this gives a very small value for λ_2 via Eq. (22). In the case of no damping ($\alpha = 0$) we have $\lambda_2 = 0$, so Eq. (21) gives $H_n \sim 1/\sqrt{\rho}$ for large ρ and thus a non-exponential decay of the magnetic configuration to the uniform state. If dissipation is present ($\alpha > 0$) then λ_2 is positive but the exponential decay would be slow so instabilities are expected.

The above described situation occurs when $h_{\text{ext}} = 0$, in which case we have $\kappa_+ \approx \omega^2 > 0$. For values of the external field $h_{\text{ext}} \gtrsim 0.01$ the numerical data show that the eigenvalue $\kappa_1 = \kappa_+$ turns negative and thus λ_2 acquires significantly larger values, that is, the decay of the magnetic configuration to the uniform state becomes fast. This behaviour of the eigenvalue κ_1 explains the great sensitivity, shown in Fig. 9, of d_{VA} on h_{ext} for very small fields $h_{\text{ext}} < 0.01$. The angular frequency, shown in Fig. 5, is correspondingly very sensitive for small h_{ext}, although this is not revealed in the scale of the figure.

We turn to study the instability indicated in Fig. 6 which shows fast rotation for smaller values of $|\beta|$ at a fixed h_{ext} and no steady states for small enough $|\beta|$. For the data shown in Fig. 6, the numerical results give $\kappa_+ < 0$. So, an increased ω, for any fixed h_{ext}, leads to values for $\kappa_1 = \kappa_+$ closer to zero according to Eq. (20). This gives $\kappa_+ = 0$ for angular frequency equal to

$$\omega_{\max} = \sqrt{h_{\text{ext}}(1 + h_{\text{ext}})}, \tag{23}$$

and we would thus expect the magnetic configuration to tend to delocalise for $\omega \gtrsim \omega_{\max}$. Indeed, Eq. (23) gives a fair approximation to the numerical results regarding the maximum angular frequency obtained for fixed $h_{\text{ext}} \gtrsim 0.1$ and no rotation faster than in Eq. (23) was obtained in numerical simulations. We conclude that the slow decay of the configuration is responsible for the unsustainability of VA dipoles at small spin torque strength.

An important lesson from the results of the asymptotic analysis is that the rate of energy dissipation for rotating VA pairs may depend greatly on the features of the magnetisation configuration. For example, a slow decaying configuration would dissipate energy much faster than a well-localised configuration. Put it another way, the rate of energy dissipation may not be proportional to the value of the dissipation constant α.

6. Uniform spin-current

The results of the previous sections showed that when the spin-torque is localised under a nano-aperture we have a favourable situation for the stabilisation of a VA pair. In this section we present

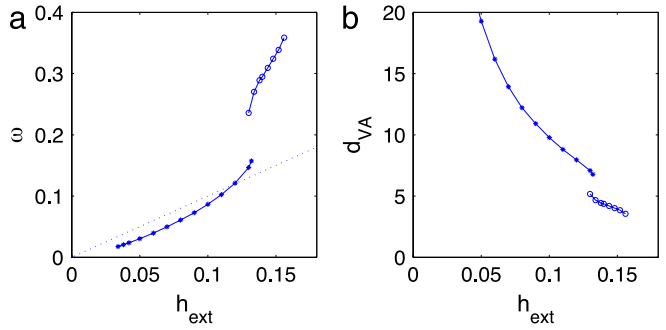

Fig. 11. (a) Angular frequency of rotation ω as a function of the applied field h_{ext}. The solid blue lines show numerical results for an uniform spin current and parameter set (24). We have two separate branches of rotating VA pairs. The lower frequency branch (long VA pairs) for $h_{\text{ext}} \leq 0.132$ and the upper branch (short VA pairs) for $0.130 \leq h_{\text{ext}} \leq 0.156$. The dotted line shows $\omega = h_{\text{ext}}$ for comparison. (b) The separation distance between vortex and antivortex as a function of applied field h_{ext}. The lower frequency branch corresponds to larger VA separation, while the upper frequency branch corresponds to smaller VA separation.

simulations and show that there are steady-state rotating VA pairs also in the case that the current flows through a large area.

We assume in this section an uniform external field (5) and an uniform spin current polarisation (4). We will present results for the parameter values

$$\alpha = 0.1, \qquad \beta = -0.05. \tag{24}$$

Simulations converge to a steady state rotating VA pair for external fields $h_{\text{ext}} \leq 0.156$.

Fig. 11 shows the rotation frequency ω and the distance d_{VA} between the vortices for parameter set (24) and for the range of values of h_{ext} where a steady state was reached. We find two separate branches of VA pairs. For $h_{\text{ext}} \leq 0.132$ we have a branch of low frequencies and large VA pair separation, which correspond to long VA pairs. The branch apparently persists for low values of h_{ext}, however, we do not present results for $h_{\text{ext}} < 0.03$ because the VA separation d_{VA} becomes very large and our numerical results are then not reliable, since the accuracy of the simulations (spatial resolution) for vortices far from the origin is inadequate. A separate branch of short VA pairs with higher frequencies and smaller VA pair separation exists for $0.130 \leq h_{\text{ext}} \leq 0.156$. For $h_{\text{ext}} > 0.156$ we find no steady state rotation (the VA pair is annihilated). For a narrow range of external fields, $0.130 \leq h_{\text{ext}} \leq 0.132$, we have two different steady states and the simulation converges to either a long or a short pair depending on the initial condition.

The Derrick relation (7) is valid here and it is indeed satisfied with an accuracy better than 1% in all our numerical simulations. It provides a guide for the expected frequencies. For short VA pairs we find $\ell \approx \mu_1$, so the angular frequency has a significant contribution from the first term on the rhs in Eq. (7) while it is linearly increasing with h_{ext} due to the second term. For long VA pairs we have $\mu_1 < \ell$, and the main contribution to ω is due to the second term which it is approximately proportional to h_{ext}.

7. Conclusions

Magnetic vortex–antivortex pairs where the vortex and antivortex have opposite polarities have skyrmion number unity, and the configuration can actually be obtained from the usual axially symmetric skyrmions by a transformation. We have studied their dynamics under the influence of spin-polarised current and external magnetic field using the Landau–Lifshitz–Gilbert–Slonczewski equation. Both the polarisation of the spin current and the magnetic field are in-plane along the same direction. Their motion is rotational and it is stabilised by the presence of a spin-torque with in-plane polarisation. The external field contributes directly to the rotation frequency and also indirectly by bringing the vortex and antivortex closer together so that they interact stronger. The rotational dynamics due to both the interaction between vortex and antivortex and the external field is linked to the skyrmion number.

When an external field is present in the Landau–Lifshitz equation we would typically expect precession of magnetisation around the field. In the case of the VA dipole we rather have rotation of the magnetisation configuration. This surprising result is due to the nonzero skyrmion number of the VA dipole.

We have studied details of the configurations which led to the identification of three types of rotating VA pairs by numerical simulations. Analytical results on the asymptotic behaviour of the rotating configurations away from the centre of the VA pair elucidate some features of the configurations and of their stability. Our extensive numerical and detailed analytical results may prove to be a necessary guide for any further observations of magnetisation oscillations due to nonlinear excitations.

An important point on the techniques employed is that the derivation of most analytical results is based on the use of the stereographic projection variable (A.1). This allows description of a VA dipole configuration via an axially symmetric ansatz, and in special cases it leads to an exact description of the dynamics.

The framework developed in the present paper can be applied to spin-transfer oscillators where the magnetisation oscillations are produced due to various external probes, i.e., due to external magnetic field and spin-torques with various combinations of polarisations. One possible direction is the oscillations of magnetic bubbles in perpendicular anisotropy materials, in an analogy to precessing droplets [26,27]. Also, the effect of perpendicularly oriented polarisers could be analysed [28].

Our main results rely upon the form of Eq. (1) but they do not depend on the specific interactions which we included. In fact, rotating VA dynamics has already been observed in full micromagnetic simulations in Ref. [5], so the magnetostatic field is not changing the general picture developed in this work.

Acknowledgements

This work was partially supported by the European Union's FP7-REGPOT-2009-1 project "Archimedes Center for Modeling, Analysis and Computation" (grant agreement no. 245749) and by grant KA3011 of the University of Crete. I am grateful to Nikos Papanicolaou for discussions and suggestions, and to Giovanni Finocchio and Dima Berkov for discussions of numerical and experimental results. I also gratefully acknowledge discussions with Dimitris Mitsoudis on Bessel functions, and with Dimitris Tsagkarogiannis.

Appendix A. Stereographic projection variable

A representation of the magnetisation vector $\boldsymbol{m}$ can be given by its stereographic projection on a plane. We define the complex variable

$$X = \frac{m_2 + i m_3}{1 + m_1}, \tag{A.1}$$

which is the stereographic projection of $\boldsymbol{m}$ from the point $\boldsymbol{m} = (1, 0, 0)$. The components of $\boldsymbol{m}$ are given as

$$m_1 = \frac{1 - X\overline{X}}{1 + X\overline{X}}, \qquad m_2 = \frac{X + \overline{X}}{1 + X\overline{X}}, \qquad m_3 = \frac{1}{i}\frac{X - \overline{X}}{1 + X\overline{X}}, \tag{A.2}$$

where $\overline{X}$ is the complex conjugate of X. This variable turns out to be particularly useful for studying many properties of the VA dipole.

For the usual conventions adopted in the present paper, we have $\boldsymbol{m}(\rho \to \infty) = (1, 0, 0) \Rightarrow X(\rho \to \infty) = 0$ while

$\boldsymbol{m}(\rho = 0) = (-1, 0, 0) \Rightarrow X(\rho = 0) \to \infty$. At the centres of the vortices we have $\boldsymbol{m} = (0, 0, \pm 1) \Rightarrow X = \pm i$.

The Landau–Lifshitz–Gilbert–Slonczewski equation of motion, when we assume external field (5) and spin polarisation (4), takes the following form

$$(i+\alpha)\,\dot{X} = \partial_\mu \partial_\mu X - \frac{2\overline{X}}{1+X\overline{X}}\,\partial_\mu X \partial_\mu X - \frac{1}{2}\,\frac{X-\overline{X}}{1+X\overline{X}}\,(1+X^2) - (h_{\rm ext} + i\beta)\,X, \tag{A.3}$$

where $\mu = 1, 2$ and summation is implied.

We can further use the complex position $z = x + iy$ on the xy-plane, denote its complex conjugate by $\bar{z}$, so we consider $X = X(z, \bar{z}, t)$. The skyrmion number is given by

$$\mathcal{N} = \frac{1}{4\pi}\int n\, d^2x, \quad n = 4\,\frac{|\partial_z X|^2 - |\partial_{\bar{z}} X|^2}{(1+X\overline{X})^2}. \tag{A.4}$$

Of particular interest here is the form

$$X = \frac{\bar{a}}{\bar{z}}, \tag{A.5}$$

where a is a complex constant and $\bar{a}$ its complex conjugate. This represents a skyrmion with $\mathcal{N} = 1$ as can be calculated using (A.5). Configuration (A.5) consists of two merons at a distance $2|a|$ apart, while each of the merons has core size $|a|$ [10]. Note that, at $z = \pm ia$ we have $m_3 = \pm 1$, so the two-meron configuration can also be viewed as a VA dipole where a vortex with negative polarity is centred at $z = -ia$ and an antivortex with positive polarity at $z = ia$. The constant $|a|$ gives the vortex core size and the distance between the vortex and the antivortex is $d_{\rm VA} = 2|a|$. More general skyrmion configurations have been studied in Ref. [10].

Appendix B. A virial relation

Motivated by the numerical results let us assume the existence of exact steady states in the model (1). More precisely, we assume a configuration rigidly rotating at an angular frequency ω, so we have

$$\dot{\boldsymbol{m}} = -\omega\,\epsilon_{\lambda\nu}\,x_\lambda \partial_\nu \boldsymbol{m}. \tag{B.1}$$

This is inserted in Eq. (1) to obtain virial (integral) relations. The procedure is developed in Ref. [21] and it is applied for the LLG equation. For an uniform magnetic field (5) and a spin-torque term with polarisation (4) a generalisation of this procedure gives a, so-called, Derrick relation [17]:

$$\omega\left(\ell + \frac{\alpha}{2}\int \epsilon_{\lambda\nu}\,x_\lambda x_\mu d_{\mu\nu}\,d^2x\right) = -\left(E_{\rm a} + h_{\rm ext}\,\mu_1 + \frac{1}{2}\int x_\mu \tau_\mu\, d^2x\right), \tag{B.2}$$

where

$$d_{\mu\nu} \equiv \partial_\mu \boldsymbol{m}\cdot\partial_\nu \boldsymbol{m}, \qquad \tau_\mu \equiv -\beta(\boldsymbol{m}\times\partial_\mu \boldsymbol{m})\cdot\boldsymbol{p} \tag{B.3}$$

and all other symbols are explained in the main body of the paper. All the integrals are understood to extend over the whole plane. The Derrick relation (B.2) is valid for all steady-state rotating solutions.

Results concerning the connection between the frequency, energy and the orbital momentum particularly for non-topological solitons for magnets with axial symmetry ware obtained in earlier works reviewed in [11,12].

Appendix C. Numerics

We simulate numerically the dynamics of the magnetisation vector $\boldsymbol{m}$ using Eq. (1). The time integration is performed by a 4th order Runge–Kutta method. The method does not preserve the length of $\boldsymbol{m}$ so we enforce unit length for $\boldsymbol{m}$ after every iteration by appropriately normalising it. We use finite differences in a lattice 251×251 and we simulate the infinite plane using stretched coordinates ξ, η [7], such that the Cartesian coordinates are given by

$$x = \frac{1}{a}\,\tan(\xi), \qquad y = \frac{1}{a}\,\tan(\eta). \tag{C.1}$$

The stretched coordinates take values in the interval $-\pi/2 \le \xi, \eta \le \pi/2$ with a uniform spacing, so that x, y extend from $-\infty$ to ∞. The coefficient a is chosen such that the spacing for x and y at the lattice centre is $\Delta x = \Delta y = 0.15$.

We typically start the simulations using one of the two following configurations. The first is the configuration in Eq. (A.5). The second is a configuration for a vortex and an antivortex, at some distance form each other, each of which is a static solution of the conservative Landau–Lifshitz equation, i.e., Eq. (1) with no dissipation, spin-torque and external field term. In the second case, we employ the stereographic variable $\Omega = (m_1 + im_2)/m_3$ and compute this for the static vortex $\Omega_V(x, y)$ and the antivortex $\Omega_{AV}(x, y)$ configuration as functions of x, y. We finally produce the vortex–antivortex ansatz $\Omega(x, y) = \Omega_V(x - a, y)\,\Omega_{AV}(x + a, y)$, where the vortex is at position $(a, 0)$ and the antivortex at $(-a, 0)$. From Ω we can compute $\boldsymbol{m}$ which is used as an initial condition in the numerical code.

The initial distance between the vortex and the antivortex is chosen in a wide range of values and we observe that this does not affect the convergence to a rotating VA pair.

We typically perform a sequence of numerical simulations sweeping a range of values for the parameters $h_{\rm ext}$ or β. The first simulation in the sequence uses the above described initial conditions while subsequent simulations use the previously found configuration as an initial condition.

References

[1] S.E. Russek, W.H. Rippard, T. Cecil, R. Heindl, Spin-transfer nano-oscillators, in: Handbook of Nanophysics, CRC Press, Honolulu, USA, 2010, pp. 1–23 (chapter 38).
[2] D.V. Berkov, N.L. Gorn, J. Appl. Phys. 99 (2006) 08Q701.
[3] D.V. Berkov, N.L. Gorn, J. Phys. D: Appl. Phys. 41 (2008) 164013.
[4] D.V. Berkov, N.L. Gorn, Phys. Rev. B 80 (2009) 064409.
[5] G. Finocchio, O. Ozatay, L. Torres, R.A. Buhrman, D.C. Ralph, B. Azzerboni, Phys. Rev. B 78 (2008) 174408.
[6] V.L. Pokrovskii, G.V. Uimin, JETP Lett. 41 (1985) 128.
[7] N. Papanicolaou, P.N. Spathis, Nonlinearity 12 (1999) 285.
[8] S. Komineas, Phys. Rev. Lett. 99 (2007) 117202.
[9] A.A. Belavin, A.M. Polyakov, JETP Lett. 22 (1975) 245.
[10] D.J. Gross, Nuclear Phys. B 132 (1978) 439.
[11] A. Kosevich, B. Ivanov, A. Kovalev, Physica D 3 (1981) 363.
[12] A.M. Kosevich, B.A. Ivanov, A.S. Kovalev, Phys. Rep. 194 (1990) 117.
[13] J. Sampaio, et al., Nature Nanotechnol. 8 (2013) 839.
[14] W.H. Rippard, M.R. Pufall, S. Kaka, S.E. Russek, T.J. Silva, Phys. Rev. Lett. 92 (2004) 027201.
[15] W.H. Rippard, M.R. Pufall, S. Kaka, T.J. Silva, S.E. Russek, Phys. Rev. B 70 (2004) 100406.
[16] M.R. Pufall, W.H. Rippard, M.L. Schneider, S.E. Russek, Phys. Rev. B 75 (2007) 140404.
[17] S. Komineas, Europhys. Lett. 98 (2012) 57002.
[18] J.C. Slonczewski, J. Magn. Magn. Mater. 159 (1996) L1.
[19] D. Berkov, J. Miltat, J. Magn. Magn. Mater. 320 (2008) 1238.
[20] R. Rajaraman, Solitons and Instantons, North Holland, Amsterdam, 1982.
[21] N. Papanicolaou, T.N. Tomaras, Nuclear Phys. B 360 (1991) 425.
[22] S. Komineas, N. Papanicolaou, Nonlinearity 11 (1998) 265.
[23] D.V. Filin, E.G. Galkina, B.A. Ivanov, JETP 97 (2013) 253.
[24] G.N. Watson, A Treatise on the Theory of Bessel Functions, Cambridge University Press, Cambridge, 1922.
[25] M. Abramowitz, I.A. Stegun, Handbook of Mathematical Functions with Formulas, Graphs, and Mathematical Tables, Dover, New York, 1965.
[26] M.A. Hoefer, T.J. Silva, M.W. Keller, Phys. Rev. B 82 (2010) 054432.
[27] S.M. Mohseni, S.R. Sani, J. Persson, T.N. Anh Nguyen, S. Chung, Ye. Pogoryelov, P.K. Muduli, E. Iacocca, A. Eklund, R.K. Dumas, S. Bonetti, A. Deac, M.A. Hoefer, J. Akerman, Science 339 (2013) 1295.
[28] T. Moriyama, G. Finocchio, M. Carpentieri, B. Azzerboni, D.C. Ralph, R.A. Buhrman, Phys. Rev. B 86 (2012) 060411.